Int. J. Electrochem. Sci., 7 **(2012)** 534 - 553

International Journal of
ELECTROCHEMICAL
SCIENCE
www.electrochemsci.org

Computational and Experimental Studies of 4-Aminoantipyrine as Corrosion Inhibitor for Mild Steel in Sulphuric Acid Solution

Acha U. Ezeoke[1], *Olalere G. Adeyemi*[1*], *Opeyemi A. Akerele*[1], *Nelson O. Obi-Egbedi* [2]

[1] Department of Chemical Sciences, Redeemer's University (RUN), Km 46, Lagos-Ibadan expressway, Redemption City, Nigeria.
[2] Department of Chemistry, University of Ibadan, Ibadan Nigeria.
[*]E-mail: drlereadeyemi@yahoo.com

Received: 11 October 2011 / *Accepted:* 1 xxx 2011 / *Published:* 1 January 2012

The inhibitive effect of 4-Aminoantipyrine (4-AAP) on the corrosion of mild steel in 0.5 M H_2SO_4 solution at 303 – 323 K was studied by weight loss measurement as well as computational techniques. Results obtained showed that 4-aminoantipyrine (4-AAP) is a good inhibitor for the corrosion of mild steel in sulphuric acid solution. The inhibition efficiency increased with 4-AAP concentration and also synergistically increased in the presence of KI and KSCN, but decreased with temperature, which is suggestive of physical adsorption mechanism. The adsorption of 4-AAP onto the mild steel surface was found to follow the Langmuir adsorption isotherm. Thermodynamics of adsorption such as enthalpy of adsorption, entropy of adsorption, equilibrium of adsorption and Gibbs free energy, were calculated and discussed. Quantum chemical calculations using DFT at the B3LYP/6-31G* level of theory was further used to calculate some electronic properties of the molecule in order to ascertain any correlation between the inhibitive effect and molecular structure of 4-aminoantipyrine.

Keywords: 4-Aminoantipyrine, Mild steel, Sulphuric acid, Langmuir isotherm, Density Functional Theory (DFT).

1. INTRODUCTION

The interaction between a metal and its environment results in the degradation of the physical and mechanical properties of the metal. Corrosion prevention and control in acidic media has been effectively achieved by the use of corrosion inhibitors. Due to environmental concern, organic inhibitors are replacing the inorganic corrosion inhibitors especially heavy metal derivatives, which have been found to be toxic to human and the environment. A number of heterocyclic compounds containing N, O, and S either in the aromatic or long chain carbon system have been reported as effective inhibitors of metal corrosion [1-3]. These inhibitors have functional groups and extended π-

electron or conjugation systems, which provide electrons that, facilitate the adsorption of the inhibitor on the metal surface. [4-7].

These polar functional groups are usually regarded as the reaction centre for the adsorption process and the resulting adsorption film acts as a barrier isolating the metal surface from the corrodent. The number, type of adsorption site on the metal surface, and the type and the extent of interaction between the organic molecule and the metal surface; determine the nature of the inhibitor adsorption [8]. The synergistic effect of halides and organic inhibitors has been reported in literature [9-11]. Halide ions have significant inhibition effect on the dissolution of mild steel in acidic media, because of their strong adsorption on the mild steel surface. The order of inhibition of halide ions on the mild steel in acid solution has been reported to be as follows: $I^- > Br^- > Cl^-$.

The present study investigates the inhibition mechanism of 4-Aminoantipyrine (4-AAP) on mild steel corrosion in 0.5 M H_2SO_4 solution at 303-323 K, using weight loss technique and quantum chemical calculations. The influence of iodide and thiocyanate ions on the adsorption and corrosion-inhibitive properties of 4-aminoantipyrine has also been studied in order to ascertain the specific mode (ionic or molecular) in which the compound exerts its inhibiting action.

2. EXPERIMENTAL TECHNIQUES

2.1 Materials

Table 1. Chemical composition of the mild steel

Element	Fe	C	Si	Mn	S	P	Ni	Cr	Mo	Cu
Composition	98.65	0.15	0.03	0.60	0.05	0.06	0.09	0.08	0.02	0.27

The composition of the mild steel [8] used in this experiment is given in Table 1 above. The sheet was mechanically pressed cut into different coupons, each of dimension 5 x 4 x 0.11 cm. Each coupon was degreased by washing with ethanol, cleaned with acetone and allowed to dry in the air before preservation in a desiccator. All reagents used for the study were Analar grade and double distilled water was used for their preparation. 0.5 M of H_2SO_4 solution was prepared for weight loss experiment. Sartorious analytical balance, model CP225D was employed in the experiment.

2.2 Inhibitor

The 4-Aminoantipyrine (4-AAP) was purchased from Sigma-Aldrich chemicals and used without further purification. To ensure proper solubility, 0.1 M stock solution of 4-AAP was made in 10:1 water : methanol mixture [18]. This stock solution was used to prepare different concentrations of 4-AAP used in this experiment. Figure 1 shows the molecular structure of 4-AAP.

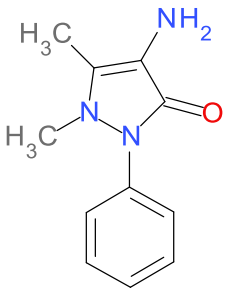

Figure 1. Molecular structure of 4-Aminoantipyrine (4-AAP)

It is evident that 4-AAP is a heterocyclic compound containing nitrogen and oxygen atoms, which could easily be protonated in acidic solution, and some π-electrons exist in this molecule. The concentration range of 4-AAP used for the weight loss experiment was $2 \times 10^{-3} - 10 \times 10^{-3}$M.

2.3. Gravimetric measurements

The gravimetric method (weight loss) is probably the most widely used method of inhibition assessment [12-15]. The simplicity and reliability of the measurements offered by the weight loss method is such that the technique forms the baseline method of measurement in many corrosion monitoring programmes [3]. Weight loss measurements were conducted under total immersion using 250 ml capacity beakers containing 200 ml test solution at 303-323 K maintained in a thermostated water bath. The mild steel coupons were weighed and suspended in the beaker with the help of rod and hook. The coupons were retrieved at 2 h interval progressively for 10 h, washed thoroughly in 20% NaOH solution containing 200 g/l of zinc dust [16] with bristle brush, rinsed severally in deionized water, cleaned, dried in acetone, and re-weighed. The weight loss, in grammes, was taken as the difference in the weight of the mild steel coupons before and after immersion in different test solutions. The tests were repeated at different temperatures. In order to get good reproducibility, experiments were carried out in triplicate. In this present study, the standard deviation values among parallel triplicate experiments were found to be smaller than 5%, indicating good reproducibility.

The corrosion rate (CR) in g cm^{-2} h^{-1} was calculated from the following equation [17]:

$$CR = \Delta W/St \quad ..... \quad (1)$$

where ΔW is the average weight loss of the three mild steel coupons after immersion, S is the total surface area of the mild steel and t is the total time of immersion which is 10 hrs.

The surface coverage and inhibition efficiency were computed using the following equations:

$$\text{Surface coverage } (\theta) = \frac{CR_{blank} - CR_{inh}}{CR_{blank}} \quad ..... \quad (2)$$

$$\text{Inhibition efficiency (\%I)} = \frac{CR_{blank} - CR_{inh}}{CR_{blank}} \times 100 \quad \ldots\ldots\ldots (3)$$

Where CR_{blank} and CR_{inh} are the corrosion rates in the absence and presence of the inhibitor respectively.

2.3 Computational details

B3LYP, a version of the DFT method that uses Becke's three-parameter functional (B3) and includes a mixture of HF with DFT exchange terms associated with the gradient corrected correlation functional of Lee, Yang, and Parr (LYP) has been recognized especially for systems containing transition metal atoms [19]. It has much less convergence problems than those commonly found for pure DFT methods. Thus, B3LYP was used in this work to carry out quantum calculations. Then, full geometry optimization of the inhibitor was carried out at the B3LYP/6-31G* level using the Spartan‟06 V112 program package.

3. RESULTS AND DISCUSSION

3.1 Effect of 4-AAP on the corrosion rate

According to the mechanism for the anodic dissolution of Fe in acid solution proposed initially by Bockris *et al* [20]. Fe electro-dissolution in acidic sulphate solutions depends primarily on the adsorbed intermediate $FeOH_{ads}$ as follows:

$$Fe + OH^- \leftrightarrow FeOH_{ads} + H^+ + e^- \quad \ldots\ldots\ldots (4)$$

$$FeOH_{ads} \rightarrow FeOH^+ + e^- \quad \ldots\ldots\ldots\ldots (5)$$

$$FeOH^+ + H^+ \leftrightarrow Fe^{2+} + H_2O \quad \ldots\ldots\ldots\ldots (6)$$

The cathodic hydrogen evolution fellows the steps:

$$Fe + H^+ \leftrightarrow (FeH^+)_{ads} \quad \ldots\ldots\ldots\ldots (6)$$

$$(FeH^+)_{ads} + e^- \leftrightarrow (FeH)_{ads} \quad \ldots\ldots\ldots\ldots (7)$$

$$(FeH)_{ads} + H^+ + e^- \leftrightarrow Fe + H_2 \quad \ldots\ldots\ldots\ldots (8)$$

The corrosion rate of iron in H_2SO_4 solutions is controlled by both hydrogen evolution reaction and dissolution reaction of iron.

Another mechanism, proposed by Ashassi-Sorkhabi and Nabavi-Amri [21] involving two adsorbed intermediates has been used to account for the retardation of Fe anodic dissolution in the presence of an inhibitor.

$$Fe + H_2O \leftrightarrow Fe \,.\, H_2O_{ads} \quad \ldots\ldots\ldots\ldots\ldots (9)$$

$$Fe \,.\, H_2O_{ads} + Y \leftrightarrow FeOH^-_{ads} + H^+ + Y \quad \ldots\ldots\ldots\ldots\ldots (10)$$

$$Fe \,.\, H_2O_{ads} + Y \leftrightarrow FeY_{ads} + H_2O \quad \ldots\ldots\ldots\ldots\ldots (11)$$

$$FeOH_{ads} \quad \_rds \quad FeOH_{ads} + e- \quad \ldots\ldots\ldots\ldots\ldots (12)$$

$$FeY_{ads} \leftrightarrow FeY^+_{ads} + e^- \quad \ldots\ldots\ldots\ldots\ldots (13)$$

$$FeOH_{ads} + FeY^+_{ads} \leftrightarrow FeY_{ads} + FeOH^+ \quad \ldots\ldots\ldots\ldots\ldots (14)$$

$$FeOH^+ + H^+ \leftrightarrow Fe^{2+} + H_2O \quad \ldots\ldots\ldots\ldots\ldots (15)$$

Where Y represents the inhibitor species.

According to the mechanism above, displacement of some adsorbed water molecules on the metal surface by inhibitor species to yield the adsorbed intermediate FeY_{ads} (equation 11) reduces the amount of the species $FeOH^-_{ads}$ available for the rate determining step. Depending on the relative solubility of the adsorbed intermediate, it could either inhibit or catalyze further metal dissolution.

The corrosion rate of mild steel in 0.5 M H_2SO_4 at different temperature in the presence and absence of the 4-AAP determined by weight loss experiment is shown in Table 2. The variation of corrosion rate with temperature for mild steel in 0.5 M H_2SO_4 at different inhibitor concentration, is shown in Figure 3. The curves show that corrosion rate increases with increasing temperature both in the absence (blank) and presence of 4-AAP. However, the corrosion rate increases more rapidly with temperature in the absence of 4-AAP.

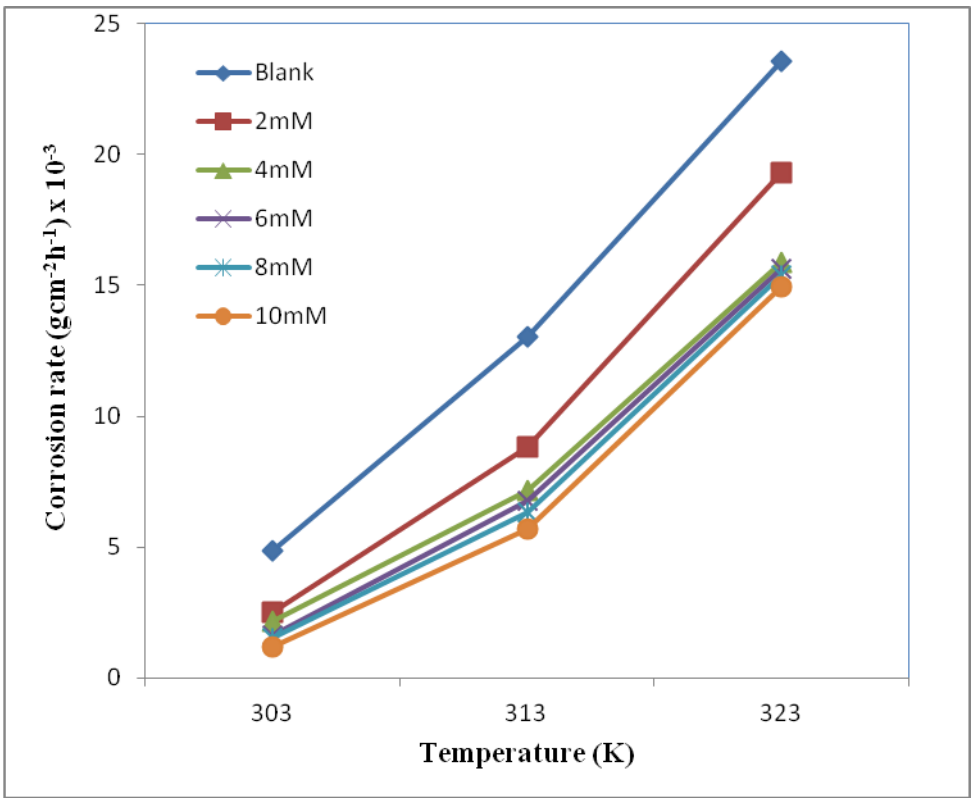

Figure 2. Relationship between corrosion rate and temperature for different concentration of 4-aminoantipyrine (4-AAP) in 0.5 M H_2SO_4

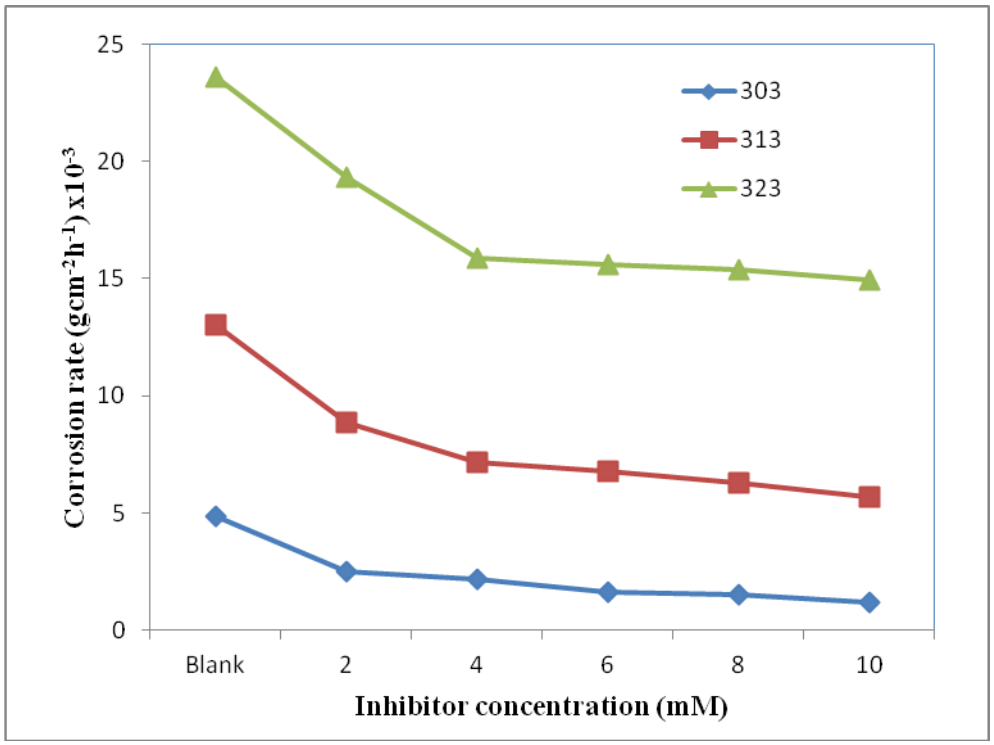

Figure 3. Relationship between corrosion rate and inhibitor concentration in 0.5 M H_2SO_4 at different temperature

Figure 2 shows the relationship between corrosion rate and system concentration for mild in the presence and absence of 4-AAP at different temperature. The curves obtained reveal that the corrosion rate decreases as the concentration of 4-aminoantipyrine (4-AAP) increases. This is due to the adsorption of 4-AAP molecules on the mild steel surface, thereby retarding the dissolution of the mild steel in the acid medium [17]. Two observations could be drawn from the results: That (a). The mild steel surface is effectively separated from the acidic medium [22, 23]. (b). 4-AAP is an efficient inhibitor for mild corrosion in 0.5 M H_2SO_4 at 303 - 323 K.

Table 2a. Calculated values of corrosion rate (CR), surface coverage (θ) and inhibition efficiency (%I) for mild steel dissolution in 0.5 M H_2SO_4 in the absence and presence of 4-aminoantipyrine at different temperature for weight loss experiment.

C onc.	303K			313K			323K		
	CR ($gcm^{-2}h^{-1}$) x 10^{-3}	θ	%I	CR ($gcm^{-2}h^{-1}$) x 10^{-3}	θ	%I	CR ($gcm^{-2}h^{-1}$) x 10^{-3}	θ	%I
Blank	4.87	-	-	13.05	-	-	23.58	-	-
2 x 10^{-3}	2.51	0.49	48.51	8.84	0.33	32.52	19.32	0.18	18.14
4 x 10^{-3}	2.17	0.55	55.43	7.18	0.45	45.19	15.88	0.33	32.65
6 x 10^{-3}	1.63	0.65	65.43	6.76	0.48	48.40	15.62	0.34	33.76
8 x 10^{-3}	1.55	0.68	68.21	6.31	0.52	51.83	15.37	0.35	34.75
10 x 10^{-3}	1.20	0.75	75.44	5.69	0.57	56.57	14.96	0.37	36.61

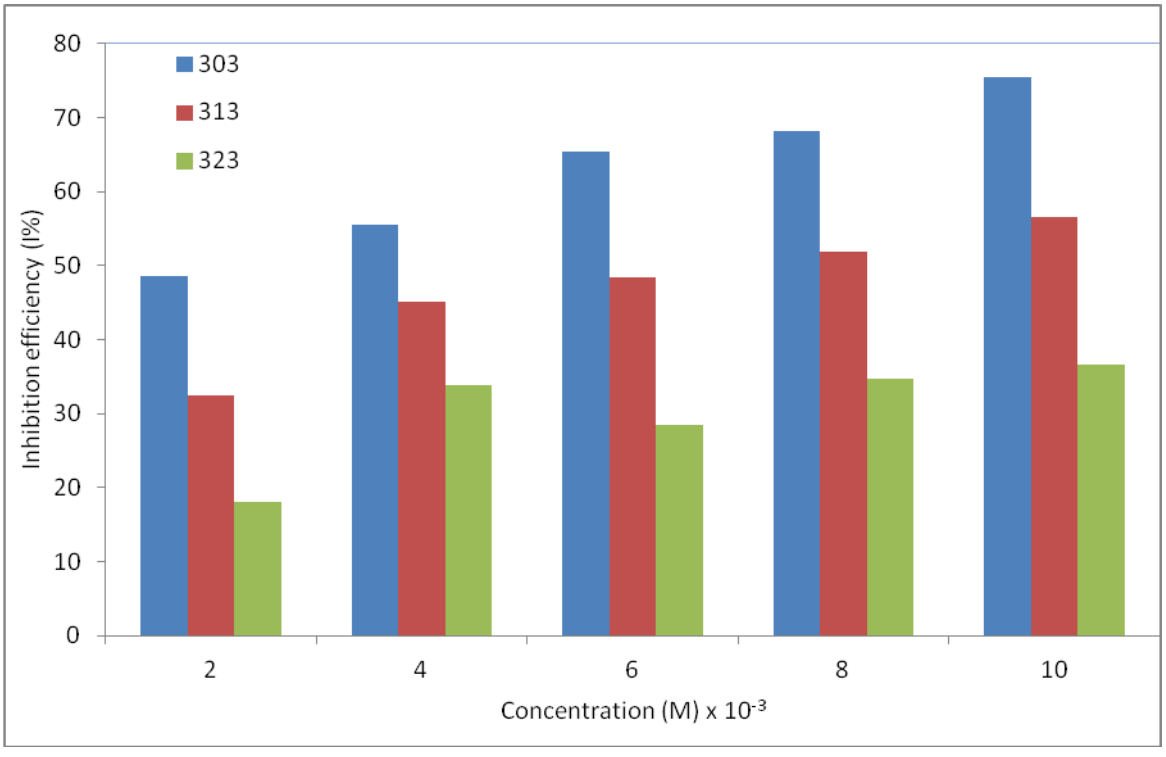

Figure 4. Relationship between Inhibition efficiency and concentration of 4-aminoantipyrine (4-AAP) at different temperature

Table 2b. Calculated values of corrosion rate (CR), surface coverage (θ) and inhibition efficiency (%I) for mild steel dissolution in 0.5 M H_2SO_4 in the presence of different concentration 4-aminoantipyrine (4-APP), KI and KSCN at different temperature

C onc.	303K			313K			323K		
	CR ($gcm^{-2}h^{-1}$) x 10^{-3}	θ	%I	CR ($gcm^{-2}h^{-1}$) x 10^{-3}	θ	%I	CR ($gcm^{-2}h^{-1}$) x 10^{-3}	θ	%I
0.005M KI	2.16	0.56	55.74	6.41	0.51	51.07	16.64	0.30	29.66
2mM AAP + KI	1.52	0.69	68.84	4.01	0.69	69.39	15.08	0.36	36.02
6mM APP + KI	1.12	0.77	77.00	2.60	0.80	80.15	9.11	0.61	61.40
10mM APP + KI	0.72	0.85	85.21	0.96	0.93	92.67	5.44	0.77	77.12
0.005 M KSCN	1.39	0.72	71.49	8.36	0.36	36.18	20.96	0.11	11.02
2mM AAP + KSCN	1.07	0.78	77.97	5.10	0.61	61.07	16.08	0.32	31.78
6mM AAP + KSCN	0.63	0.87	87.10	2.26	0.83	82.75	9.79	0.59	58.52
10mM AAP + KSCN	0.38	0.92	92.22	1.52	0.88	88.40	7.41	0.69	68.64

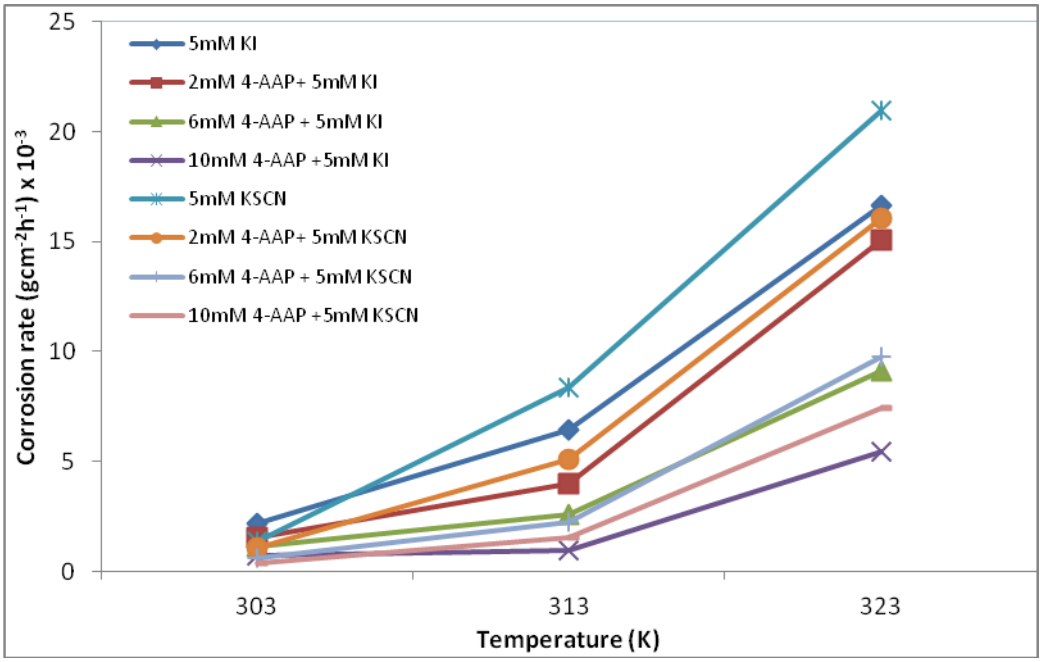

Figure 5. Relationship between corrosion rate and temperature for 0.005 M KI and 0.005 M KSCN in different concentration of 4-aminoantipyrine (4-AAP)

3.2 Effect of 4 –aminoantipyrine (4-AAP) concentration and temperature on the Inhibition efficiency.

The plot of inhibition efficiency against inhibitor concentration for the corrosion of mild steel in 0.5 M H_2SO_4 solution is given in Figure 4 above. The Figure reveals that inhibition efficient increases with increase in concentration of 4-AAP. The maximum of 75.44% was obtained for 10 $x10^{-3}$ M 4-AAP at 303 K while 2 x 10^{-3} M 4-AAP gave the least inhibition efficiency at same temperature. This observation could be attributed to the increase in the amount of 4-AAP molecules adsorbed on the metal surface, which separate the mild steel from the acidic solution. Also, the Figure shows that

inhibition efficiency decreases with increasing temperature. For all concentrations of 4-AAP, the systems at 323 K gave least efficiencies. The minimum efficiency of 18.14% was obtained for 2 $x10^{-3}$ M 4-APP at 323 K. This decrease in inhibition efficiency with temperature might be due the weakening of adsorption strength at high temperature, resulting in desorption rather than adsorption [18].

3.3 Effect of temperature and activation parameters on inhibition efficiency

Thermodynamic and activation parameters play important role in understanding the inhibitive mechanism.

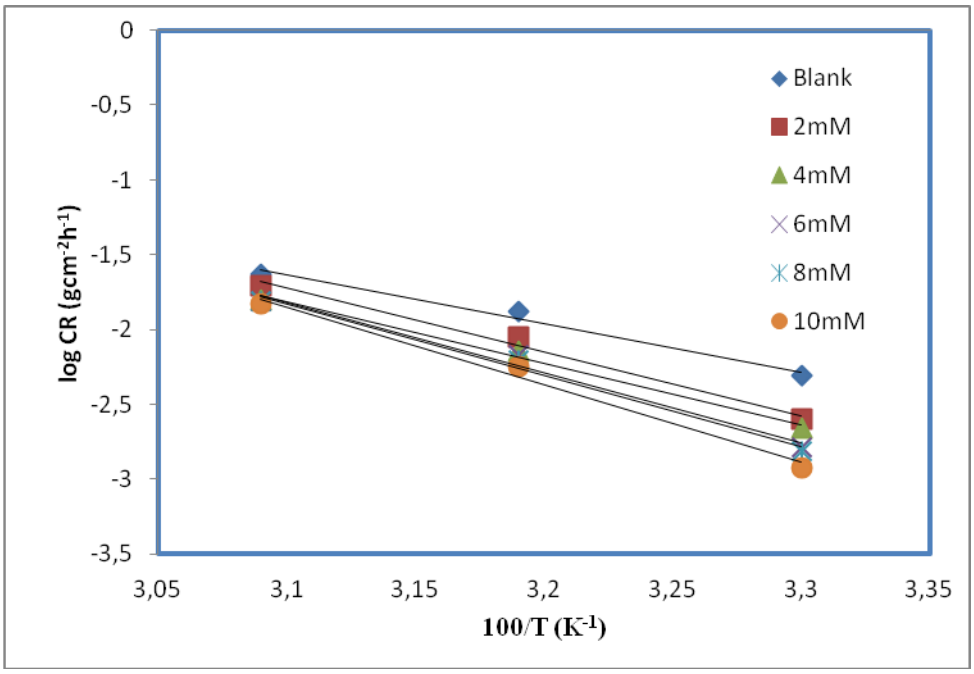

Figure 6. Arrenhuis plot for the dissolution of mild steel in 0.5 M H_2SO_4 in the absence and presence of different concentration of 4-aminoantipyrine (4-AAP).

The weight loss measurements were conducted in the temperature range of 303-323 K at an interval of 10 K, in the absence and presence of different concentrations of 4-aminoantipyrine (4-AAP) in 0.5 M H_2SO_4 for mild steel. The dependence of corrosion rate (CR) of mild steel in acid media on temperature (T) can be expressed by Arrenhius equation [24, 25].

$$\log CR = \log A - E_a/2.303RT \quad \ldots\ldots\ldots\ldots\ldots \quad (16)$$

where CR is the corrosion rate, E_a is the apparent activation energy, R is the molar gas constant (8.314 J K^{-1} mol^{-1}), T is the absolute temperature, and A is the frequency factor. The plot of log CR against 1/T for mild steel corrosion in 0.5 M H_2SO_4 in the absence and presence of different

concentrations of 4-AAP is presented in Figure 6. Table 3 below shows the calculated values of the activation parameters for mild steel in 0.5 M H_2SO_4 in the presence and absence of different concentration of 4-AAP.

Table 3. Activation parameters for the dissolution of mild steel in 0.5 M H_2SO_4 in presence and absence of different concentration of 4-aminoantipyrine (4-AAP)

C (M)	E_a (J/mol)	ΔH* (J/mol)	ΔS* (J/mol/K)	A ($gcm^{-1}hr^{-1}$)
Blank	62.21	59.45	-104.95	2.7 2 x 10^{8}
2 x10^{-3}	81.38	78.64	-162.73	2.82 x 10^{11}
4 x 10^{-3}	78.60	76.78	-155.23	8.13 x 10^{10}
6 x 10^{-3}	89.65	86.91	-186.53	4.90 x 10^{12}
8 x 10^{-3}	91.41	88.67	-191.85	9.33 x 10^{12}
10 x 10^{-3}	99.66	97.84	-220.00	1.91 x 10^{14}

Activation energy values, E_a was calculated from the slope of the plots of Figure 6 and are given in Table 3, for the blank and different inhibitor concentration. The activation energies calculated from equation 16 were found to range from 81.38J/mol to 99.66J /mol. The values are higher than 62.21J/mol obtained for the blank, indicating that 4-AAP retarded the corrosion of mild steel in 0.5 M H_2SO_4. It is also an indication of a strong inhibitive action of 4-AAP by increasing energy barrier for the corrosion process, emphasizing the electrostatic character of the inhibitor's adsorption on the mild steel surface (physisorption) [26]. The activation energies were also found to be lower than the threshold value of 80kJ/mol required for the mechanism of chemical adsorption. Therefore the adsorption of 4-AAP on mild steel surface obeys the mechanism of physical adsorption [27].

To calculate the enthalpy of adsorption ΔH^*_{ads} and the entropy of adsorption ΔS^*_{ads}, equation (17) called the transition state equation was employed.

$$CR = (RT/Nh) \exp(\Delta S^*/R) \exp(-\Delta H^*/RT) \quad \text{---------- (17)}$$

Where CR is the corrosion rate, R is the molar gas constant, T is the absolute temperature, h is the Planck's constant and N is the Avogadro's number. Plots of log (CR/T) against 1/T (Figure 7) gave straight lines with slope of (-ΔH*/2.303R) and intercept of (log R/Nh + ΔS*/2.303R) from which the values of ΔH* and ΔS* listed in Table 3 were calculated. Table 3 reveals that ΔH* gave positive values which reflect the endothermic nature of the dissolution of mild steel in 0.5 M H_2SO_4. The values of ΔS* in the presence and absence of the 4-AAP are negative, because inhibitor molecules were not constrained and freely moving in the bulk solution (inhibitor molecules were chaotic), were adsorbed in an orderly fashion onto the mild steel surface resulting to decrease in entropy [27]. Also the negative values of ΔS* indicate that the activation complex in the rate determining step represents association rather than dissociation. This implies a decrease in disorder on going from reactants to the activated complex [26].

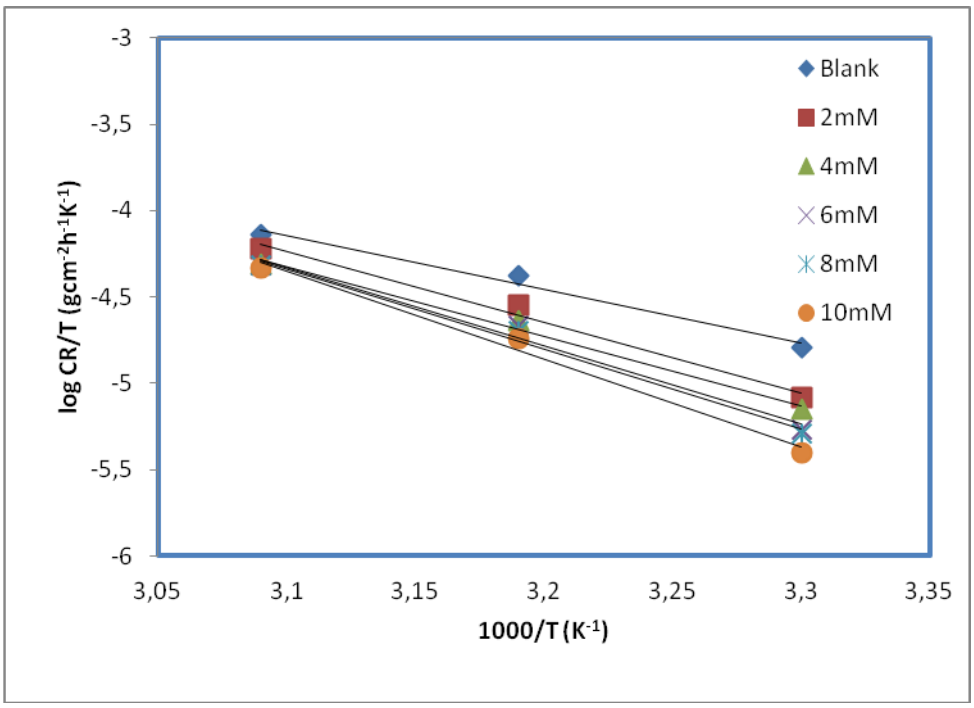

Figure 7. Transition state plot for the dissolution of mild steel in 0.5 M H_2SO_4 in the presence and absence of different concentration of 4-aminoantipyrine (4-AAP)

3.4 Adsorption considerations

The adsorption of inhibitor molecules from aqueous solutions can be regarded as a quasi-substitution process between the organic compound in the aqueous phase Org (aq) and water molecules at the electrode surface, $H_2O(s)$.

$$Org\ (aq.) + x\ H_2O\ (s) \rightarrow Org\ (s) + x\ H_2O\ (aq) \quad \text{---------- (18)}$$

where x, the size factor, is the number of water molecules displaced by one molecule of organic inhibitor. Adsorption isotherms are very important in determining the mechanism of organoelectrochemical reactions [26]. The surface coverage (ɵ) for the inhibitor was obtained from the weight loss measurement for various concentrations of 4-AAP at different temperatures (303-323K), as shown in Table 2. It is important to determine empirically which adsorption isotherm fits best to the surface coverage data in order to use the corrosion rate measurements to calculate the thermodynamic parameters pertaining to inhibitor adsorption. The most frequently used isotherms are Langmiur, Frumkin, Freundlich, Hill de Boer, Parsons, Temkin, Flory-Huggins and Dahar-Flory-Huggins and Bockris-Swinkel [28-32]. All these isotherms are of the general form: $f(ɵ,x)\exp(2aɵ) = KC$

In this work the models considered were

$$\text{Temkin isotherm: } \exp(fɵ) = K_{ads}C \quad \text{---------- (19)}$$

Langmuir isotherm: $\theta/1-\theta = K_{ads}C$ ---------- (20)

Frumkin isotherm: $\theta/1-\theta \exp(-2f\theta) = K_{ads}C$ ---------- (21)

Freundlich isotherm: $\theta = K_{ads}C$ ---------- (22)

Where K_{ads} is the equilibrium constant of the adsorption process. C is the inhibitor concentration and f the factor of energetic inhomogeneity. The best-fitted straight line is for the plot of C/θ against C (Figure 8). The correlation coefficient (R^2) was used to choose the isotherm that best fit the experimental data (Table 2). This suggests that the adsorption of 4-AAP on mild steel surface obeyed Langmuir adsorption isotherm.

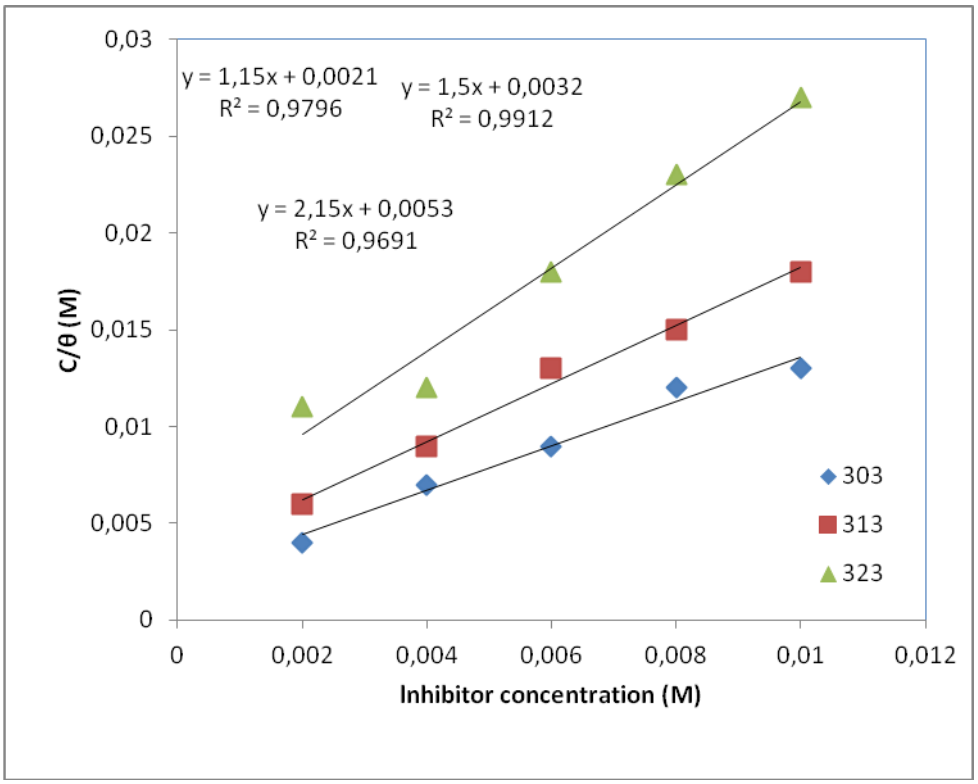

Figure 8. Langmuir plot for mild steel dissolution in 0.5 M H_2SO_4 in presence of 4-AAP at different temperature

The Langmuir adsorption isotherm model has been used extensively in the literature for various metal, inhibitor and acid solution systems [9,12,16,25]. The plot of C/θ against C (Figure 8), using equation (23), yielded a straight line with $R^2 = 0.991$.

$$C_{inh}/\theta = 1/K_{ads} + C_{inh} \quad \text{---------- (23)}$$

Where C_{inh} is the inhibitor concentration and K_{ads} is the equilibrium constant for the adsorption or desorption process. From the intercepts of the straight lines on the C_{inh}/θ axis, K_{ads} is calculated, which is related to the standard free energy of adsorption, ΔG_{ads}, as given by equation 24 [25].

$$\Delta G_{ads} = -2.303RT \log(55.5K_{ads}) \quad \text{----------} \quad (24)$$

Where R is the molar gas constant, T is the system temperature measured in (K) and 55.5 is the concentration of H_2O molecules.

Calculated values of free energies (ΔG_{ads}) are given in Table 4; the negative values of ΔG_{ads} indicate spontaneous adsorption of 4-AAP onto the mild steel surface [4] and strong interactions between inhibitor molecules and the metal surface [33]. Generally, values of ΔG_{ads} up to -20kJmol^{-1} are consistent with physisorption, while those around -40kJmol^{-1} or higher are associated with chemisorptions, which is as a result of the sharing or transfer of electrons from organic molecules to the metal surface to form a coordination compound [4]. In this work, the calculated values of ΔG_{ads} were higher than -20kJmol^{-1} but less than -40kJmol^{-1}, indicating mixed adsorption but physisorption being the dominant adsorption mechanism.

Table 4. Some parameters from Langmuir isotherm model for mild steel in 0.2 M H_2SO_4 in the presence of 4-aminoantipyrine (4-AAP) at different temperature

Temperature (K)	Slope	K_{ads} (M)	R^2	ΔG_{ads} (kJ/mol)
303	1.15	5.0 x 10^2	0.979	-25.78
313	1.50	3.3 x 10^2	0.991	-25.57
323	2.15	2.0 x 10^2	0.969	-25.02

From Table 4, it is evident that values obtained for the slope are more than unity, proposed by Langmuir. This indicates that each molecule of the 4-AAP involved in the adsorption process is attached to more than one active site on the metal surface. The values of K_{ads} decrease with increase in temperature signifying that 4-AAP was physically adsorbed on the mild steel surface. Generally, K_{ads} denotes the strength between adsorbate and adsorbent. Large values of K_{ads} indicate more efficient adsorption and hence better inhibition efficiency [34]. Higher values of K_{ads} at 303 K implies that more 4-AAP was adsorbed onto the mild steel surface leading to greater surface coverage and hence better protection efficiency than at 323 K.

3.5 Effect of KI and KSCN additives on the Inhibition efficiency

It is generally accepted that the presence of mainly halide ions in acidic media synergistically increase the inhibition efficiency of most organic compounds. These ions improve the adsorption of the organic cations by forming intermediate bridges between the positively charged metal surface and the positive end of the organic inhibitor. In other words, corrosion inhibition synergism results from

increased surface coverage arising from ion-pair interactions between the organic cations and anions [10].

Figure 5 shows the relationship between corrosion rate and temperature for 0.005 M KI and 0.005 M KSCN in different concentration of 4-aminoantipyrine (4-AAP). It can be seen that blank KI and KSCN gave lower corrosion rate at all temperature, when compared with blank H_2SO_4 solution. Also the corrosion rates were further reduced in the mixture of different concentration of 4-AAP and the additives. This suggests that both additives (KI and KSCN) synergistically reduce the dissolution of mild steel in 0.5 M H_2SO_4. Table 2b shows calculated values of corrosion rate (CR), surface coverage (ɵ) and inhibition efficiency (%I) for mild steel dissolution in 0.5 M H_2SO_4 in the presence of different concentration of 4-aminoantipyrine (4-AAP), KI and KSCN at different temperature. It is obvious from Table 2b, that the additives (KI and KSCN), synergistically increased the inhibition efficiency. The maximum efficiency of 75.44% for 10 mM of 4-AAP at 303 K was significantly increased in the presence of 0.005 M KI and 0.005 M KSCN to 85.21% and 92.22% respectively. It can also be observed that SCN^- gave better synergistic effect at lower temperature (303 K) while I^- gave greater influence at higher temperatures (313 K & 323 K). This could be attributed to the large ionic radius, high hydrophobicity, and low electronegativity of iodide ion, compared to thiocyanate ion [35,36].

Wu *et al.* [37] proposed the mechanism to account for the effect of iodide ions in improving the inhibition efficiency of benzotriazole on corrosion of copper in sulfuric acid solution. According to their proposed mechanism, the observed synergistic effect results from increased surface coverage arising from ion-pair interactions between I^- or SCN^- ions and 4-AAP cations. The ion pairs could be formed in the bulk solution and then adsorbed from the solution onto the metal surface as follows:

$$X^-_s + AAP^+_s \rightarrow (X^- - AAP^+)_s \quad \ldots\ldots\ldots\ldots\ldots (25)$$

$$(X^- - AAP^+)_s \rightarrow (X^- - AAP^+)_{ads} \quad \ldots\ldots\ldots\ldots\ldots .. (26)$$

Other corrosion researchers [38-41] proposed that, ion-pair formation could result from initial contact adsorption of the iodide ions or thiocyanate ions on the metal surface, which leads to a recharging of the electrical double layer. The inhibitor is attracted onto the double layer by the adsorbed anions such that ion-pair formation occurs directly on the metal surface.

$$X^-_s \rightarrow X^-_{ads} \quad \ldots\ldots\ldots\ldots (27)$$

$$X^-_{ads} + AAP^+_{ads} \rightarrow (X^- - AAP^+)_{ads} \quad \ldots\ldots\ldots\ldots .. (28)$$

Where X^-_s , AAP^+_s, and $(X^- - AAP^+)_s$ represent the I^- or SCN^- ion, the inhibitor, and the ion pair respectively, in the bulk of the solution, while X^-_{ads}, AAP^+_{ads}, and $(X^- - AAP^+)_{ads}$ refer to the species in the adsorbed state.

3.6 Quantum chemical studies

Quantum chemical calculations are recently used to correlate the effectiveness of an inhibitor to molecular electronic structure [7]. There has been increasing use of the density functional theory (DFT) methods in applications related to organic and bioorganic compounds [42]. In this present investigation, quantum chemical calculation using DFT was used to explain the experimental results obtained in this study and to further give insight into the inhibition action of 4-AAP on the mild steel surface.

Figures 9-13 show the optimized geometry of in neutral and in protonated form, the HOMO density distribution, the LUMO density distribution, and the Mulliken charge population analysis for 4-AAP molecule obtained with DFT at B3LYP/6-31G* level of theory. Table 4 shows the calculated quantum chemical properties for 4-AAP.

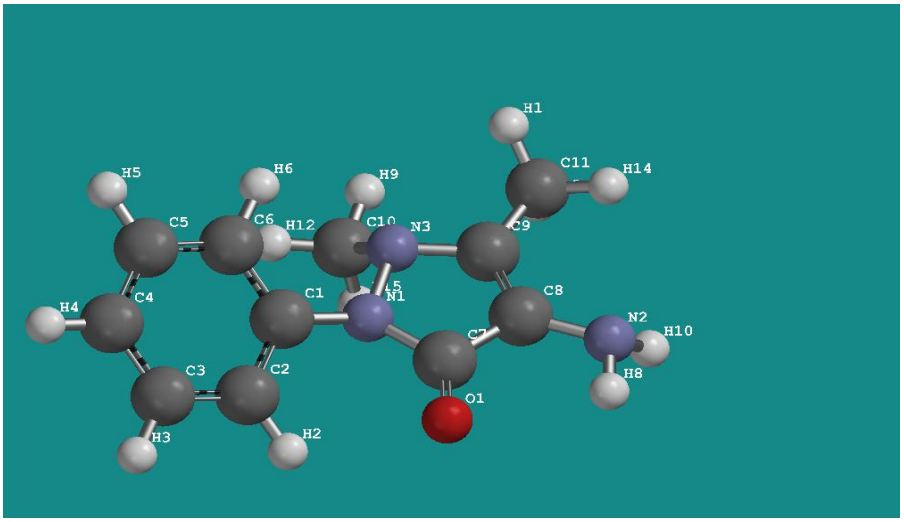

Figure 9. Optimized structure of neutral 4-aminoantipyrine (4-AAP) in aqueous solution

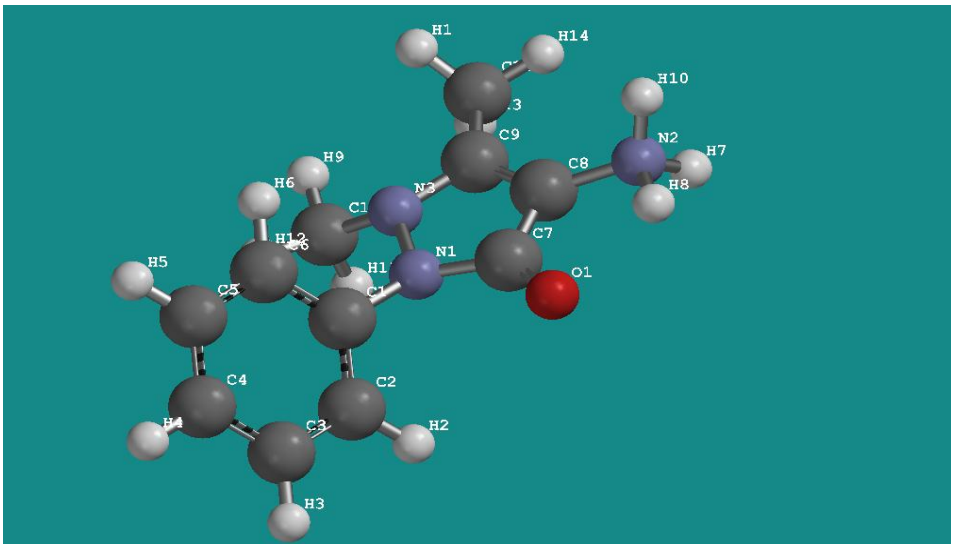

Figure 10. Optimized structure of protonated 4-aminoantipyrine (4-AAP) in aqueous solution.

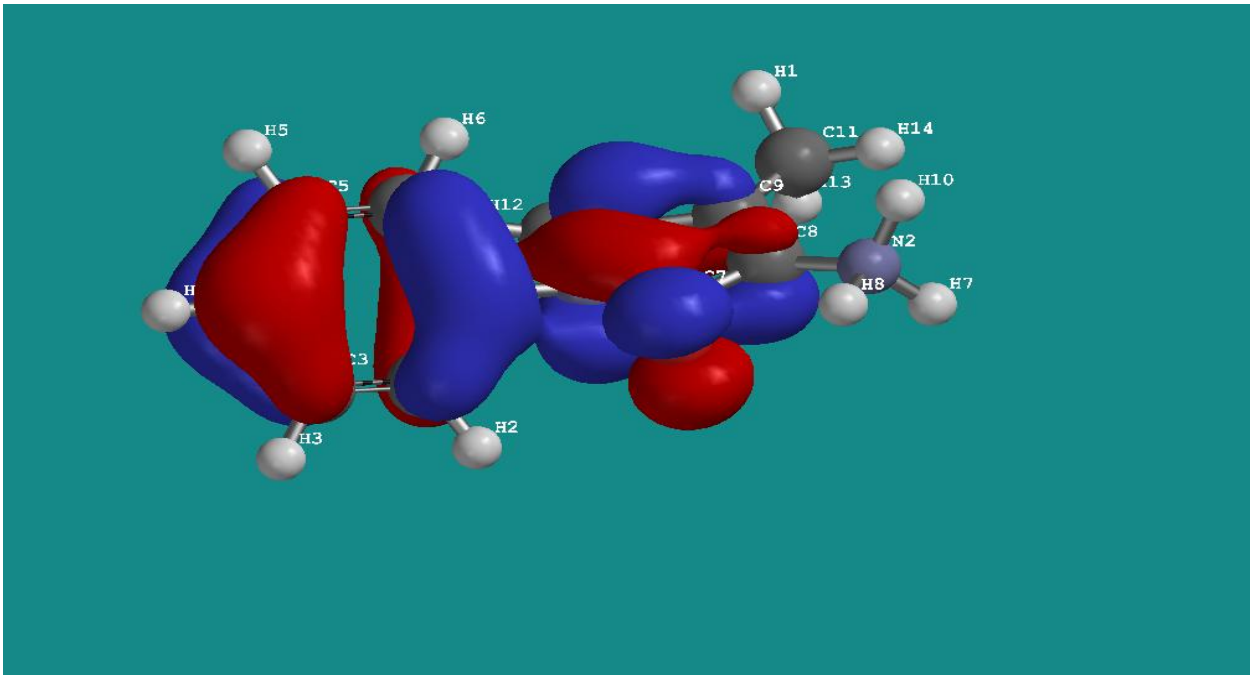

Figure 11. The (HOMO) density of protonated 4- aminoantipyrine (4-AAP) using DFT at the B3LYP/6-31G* basis set level.

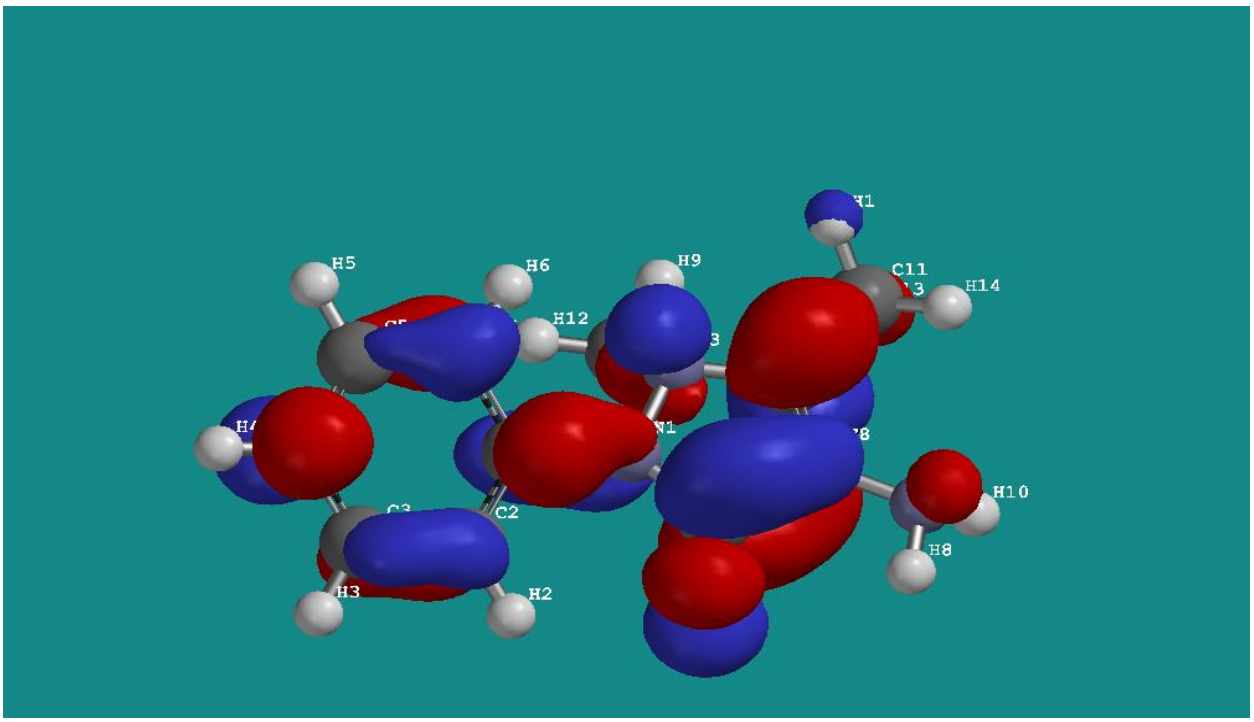

Figure 12. The (LUMO) density of 4-aminoantipyrine (4-AAP) using DFT at the B3LYP/6-31G* basis set level.

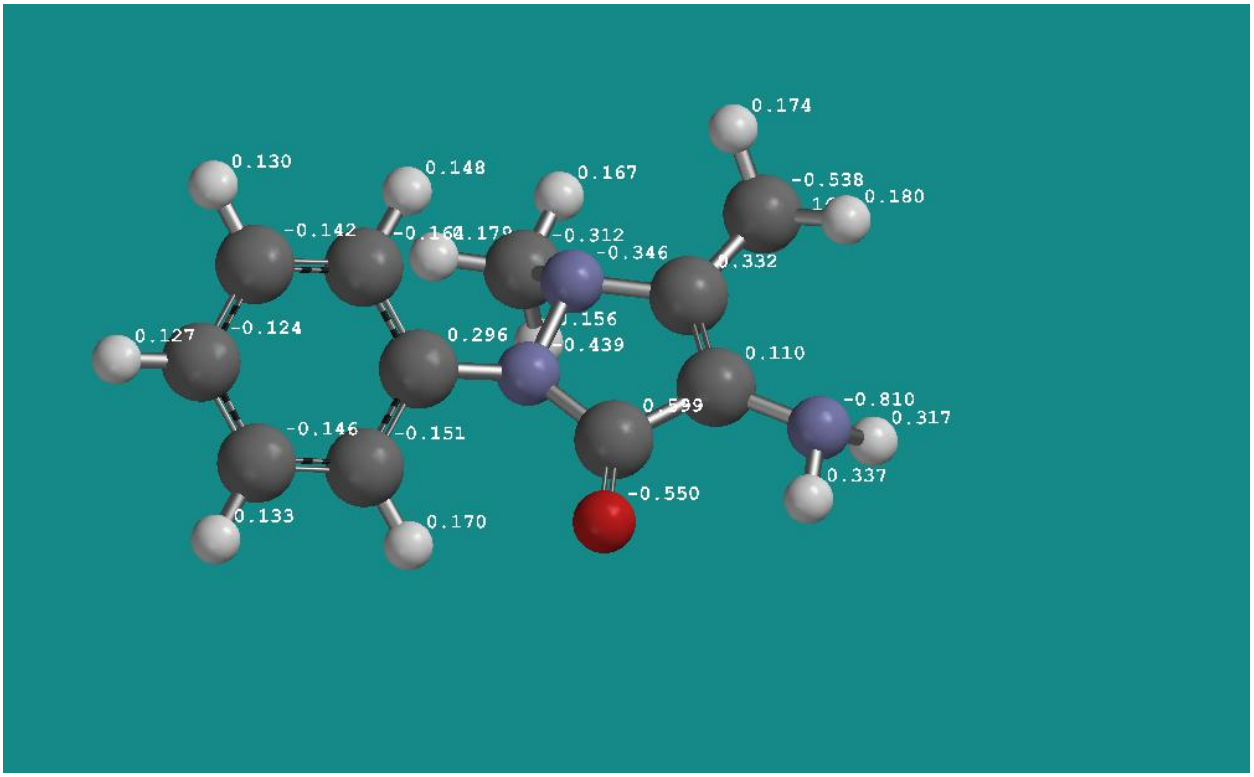

Figure 13. Mulliken charges population analysis of 4-aminoantipyrine (4-AAP) using DFT at the B3LYP/6-31G* basis set level.

Table 5. Optimized DFT parameters at the B3LYP/6-31G* level for 4-Aminoantipyrine (4-AAP)

Heat of Formation (a.u)	**-666.465088**
E_{HOMO} (eV)	-5.31791911
E_{LUMO} (eV)	-0.51203158
ΔE (E_{LUMO}- E_{HOMO})(eV)	4.8058875
Molecular weight (amu)	203.24
Dipole moment (D)	4.26
Cosmo Area ($Å^2$)	234.16
Cosmo Volume ($Å^3$)	214.45

According to frontier orbital theory, the reaction of reactants mainly occurred on the highest occupied molecular orbital (HOMO) and lowest unoccupied molecular orbital (LUMO). The energy of HOMO (E_{HOMO}) is related to ionization potential while the energy of LUMO (E_{LUMO}) is directly related to electron affinity. Higher values of E_{HOMO} indicate a tendency of the inhibitor molecules to donate electrons to appropriate acceptor molecules with low energy or empty 3d orbital of Fe to form coordinate bond [19]. The lower the values of E_{LUMO}, the stronger the electron accepting ability of the inhibitor molecule, so that back-donating bond can be formed with its anti-bonding orbitals.

Table 6. Mulliken charge of the various atoms present in 4-Aminoantipyrine (4-AAP)

Atom	Mulliken Charge
C1	0.29628
C2	-0.15080
C3	-0.14567
C4	-0.12399
C5	-0.14228
C6	-0.164183
C7	0.59914
C8	0.109631
C9	0.33231
C10	-0.31158
C11	-0.53849
N1	-0.439385
N2	-0.810142
N3	-0.34581
O2	-0.55049

From Table 5, the high value of dipole moment probably increases the adsorption between chemical compound and metal surface [43]. The adsorption of 4-AAP molecules from the aqueous solution can be regarded as a quasi-substitution process between the 4-AAP in the aqueous phase [4-$AAP_{(sol)}$] and water molecules at the electrode surface [$H_2O_{(ads)}$]. Moreover, a smaller energy gap, ΔE (E_{LUMO}-E_{HOMO}) of 4.805 (eV), a higher molecular weight, higher area and volume enhance effective adsorption of 4-AAP on the mild steel surface thus decreasing the corrosion rate of the mild steel. The Mulliken charges of the atoms in 4-AAP molecule, is shown in Figure 13 and Table 6. It has been reported elsewhere in literature, that the more the negative charge of the adsorbed centre, the more the ease for the atom to donate its electrons to the vacant 3d orbital of the metal [19,44].

From Table 6, it can be seen that, N2, N1, N3, O2 and C11 were the atoms with excess negative charges. Atom N2 has the largest negative charge, and is found in the heterocyclic ring. This implies that, the total electron density is located around these atoms. Therefore, the adsorption of 4-AAP molecules on mild steel would take place through the heterocyclic ring, the carbonyl and amine functional groups.

4. CONCLUSIONS

4-Aminoantipyrine acted as a good inhibitor for the corrosion of mild steel in 0.5 M H_2SO_4 solution. Inhibition efficiency increased with increase in inhibitor concentration but decreased with increase in temperature. The value of apparent activation energy increased with the increase in the inhibitor concentration. Enthalpy of activation reflects the endothermic nature of the mild steel dissolution process. The adsorption of 4-Aminoantipyrine (4-AAP) on the mild steel follows the

Langmuir isotherm model. Gibbs free energy of adsorption, heat of adsorption and entropy of adsorption indicated that the adsorption process is spontaneous, and the molecules are adsorbed on the metal surface by the process of physical adsorption. The stabilization of the adsorbed Iodide ion and thiocyanate ion by the adsorbed 4-AAP cations leads to greater surface coverage and consequently higher inhibition efficiency.

The introduction of 4-AAP into 0.5 M H_2SO_4 solution results in the formation of a protective film on the mild steel surface, which may contain the complex of AAP-Fe^{2+}, and effectively protects the mild steel from corrosion. Computational studies using DFT suggest that adsorption of 4-AAP on the mild steel surface would take place through nitrogen atoms in the heterocyclic ring, the carbonyl and amine functional groups.

ACKNOWLEDGEMENT
The authors acknowledged the Department of Chemical Sciences, Redeemer's University (RUN) for providing the facilities used for this research.

References

1. S. Martinez, *Mater. Chem. Phys.* 77 (2002) 97.
2. A.Popova, M. Christov, S. Rachieva, E. Sokolova, *Corros. Sci.*, 46 (2004) 1333.
3. I.B. Obot, N. O. Obi-Egbedi, S. A. Umoren, *Int. J. Electrochem. Sci.* 4 (2009) 863.
4. S. A. Umoren, I. B. Obot, E. E. Ebenso, N. O. Obi-Egbedi, *Int. J. Electrochem. Sci.* 3 (20080 1325.
5. E. S. Ferreira, C. Giacomelli, F. C. Gicomelli, A. Spinelli, *Mater. Chem. Phys.* 83 (1) (2004) 129.
6. M. Abdallah, *Corros. Sci.* 44 (2002) 717.
7. H. Ashassi-Sorkhabi, B. Shaabani, D. Seifzadeh, *Electrochimica Acta.* 50 (2005) 3446.
8. N. Hackerman, Transactions from meeting of Electrochemistry section of the New York Academy of Science, Oct. 5 (1954) 7.
9. P. C. Okafor, Y. Zheng, *Corros. Sci.* 51 (2009) 850.
10. E. E. Oguzie, Y. Li, F. H. Wang, *J. of Colloid Interf. Sci.* 310 (2007) 90.
11. G. Mu, X. Li, *J. Colloid lnterf. Sci.* 289 (2005) 184.
12. S. A.Umoren, M. M. Solomon, I. I. Udousoro, A. P. Udoh, *Cellulose* 17(3) (2010) 635.
13. M. M. Solomon, S. A. Umoren, I. I. Udousoro, A. P. Udoh, *Corros. Sci.* 52(4).
14. S. A. Umoren, I. B. Obot, N. O. Obi-Egbedi, *Desalination,* 247 (2009) 561.
15. E. E. Oguzie, G. N. Onuoha, *Mater. Chem. Phys.* 89 (2005) 30.
16. I.B. Obot, N. O. Obi-Egbedi, S. A. Umoren, *Int. J. Electrochem. Sci.* 4 (2009) 863.
17. E. E. Ebenso, I. B. Obot, *Int. J. Electrochem. Sci.* 5 (2010) 2012.
18. K. F. Khaled. *Electrochim. Acta,* 3 (2008) 3484.
19. I.B. Obot, N. O. Obi-Egbedi, *Mater. Chem. Phys.* 122 (2-3) (2010) 325.
20. J. OM Bockris, D. Drazic, A. R. Despic, *Electrochimica Acta.* 4 (1961) 325.
21. H. Ashassi-Sorkhabi, S. A. Nabavi-Amri, *Acta. Chimica Slov.* (200) 507.
22. X. Li, S. Deng, H. Fu, G. Mu, *Corros. Sci.* 51 (2009) 620.
23. T. P. Zhao, G. N. Mu, *Corros. Sci.* 41 (1999) 1937.
24. P. B. Mathur, T. Vasudevan, *Corros. Sci.* 38 (1982) 17.
25. S. M. Abd El-Haleem, A.A. Abdel Fattah, W. Tayor, *Res. Mech.* 30(3) (1985) 333.
26. M. Abdallah, E. A. Helal, A. S. Founda, *Corros. Sci.* 48 (2006) 1639.
27. H. Rehan, *Material wissenschaft & Werksofftechnik* 34(2) (2003) 232.

28. B.B. Damaskin, B. Batraktov, Adsorption of organic compds on Electrodes, *Plenum Press,* New York, 1971.
29. I.Langmuir, *J. Am. Chem. Soc.* 39 (1917) 1848.
30. H. Dhar, B. Conway, K. Joshi, *Electrochim. Acta,* 18 (1973) 789.
31. A.N. Frumkin, *J. Phys. Chem.* 116 (1925) 466.
32. O. Ikeda, H. Jimbo, H. Tamura, *J. Electroanal. Chem.* 137 (1982) 127.
33. U. J. Ekpe, E. E. Ebenso, U. J. Ibok, *J. W. Afri. Sci. Assoc.* 37 (1994) 13.
34. S. Refaey, F. Taha, A. M. Abd El-Malak, *Appl. Surf. Sci.* 236(2004) 175.
35. E. E. Oguzie, G. N. Onuoha, A. I. Onuchukwu, *Mater. Chem. Phys.* 89 (2004) 305.
36. Y. I. Kuznetsov, N. N. Andreev, *Corrosion 96, NACE International,* Houston paper No. 214.
37. Y. C. Wu, P. Zhang, H. W. Pickering, D. L. Allara, *J. Electrochem. Soc.* 140 (1993) 2971.
38. E. E. Oguzie, *16th International Corrosion Congress Beijing, China.* 2005, paper 17-45.
39. E. E. Oguzie, C. Unaegbu, C. N. Ogukwe, B. N. Okolue, A. I. Onuchukwu, *Mater. Chem. Phys.* 84 (2004) 363.
40. E. E. Oguzie, *Mater. Chem. Phys.* 87 (2004) 212.
41. M. El Azhar, B. Mernari, M. Traisnel, F. Bentiss, M. Lagrenee, *Corros. Sci.* 43 (2001) 2229.
42. G. Gao, C. Liang, Electrochim. Acta. 52 (2007) 4554.
43. S. Vijayakumar, P. Kolandaivel, J. Mol. Struct. (THEOCHEM) 770 (2006)23.
44. I.B. Obot, N. O. Obi-Egbedi, Corros. Sci. 51(2009) 276.